5420 *Chem. Mater.* **2010,** *22,* 5420–5429
DOI:10.1021/cm1001708

CHEMISTRY OF MATERIALS
Article

Magnetic properties of Zn-substituted $MnFe_2O_4$ nanoparticles synthesized in polyol as potential heating agents for hyperthermia. Evaluation of their toxicity on Endothelial cells

Z. Beji,[†,‡] A. Hanini,[†,§,⊥] L.S. Smiri,[‡] J. Gavard,[§] K. Kacem,[⊥] F. Villain,[||] J.-M. Grenèche,[#] F. Chau,[†] and S. Ammar*[,†]

[†]*Interface Traitement, Organisation et Dynamique des Systèmes, Université Paris 7, UMR-CNRS 7086, 75205 Paris, France,* [‡]*Unité de Recherche de Chimie Inorganique et Structurale, 99UR/12-30, Faculté des Sciences de Bizerte, 7021 Zarzouna, Tunisia,* [§]*Institut Cochin, Université Paris Descartes, UMR-CNRS 8104, U-INSERM 1016, Paris, France, INSERM, U1016, Paris, France,* [⊥]*Laboratoire de Physiologie Intégrée, Faculté des Sciences de Bizerte, 7021 Zarzouna, Tunisia,* [||]*Laboratoire de Chimie Inorganique et des Matériaux Magnétiques, Université Paris 6, UMR-CNRS 7071, 75251 Paris, France, and* [#]*Laboratoire de Physique de l'Etat Condensé, Université du Maine, UMR-CNRS 6087, 72085 Le Mans, France*

Received January 20, 2010. Revised Manuscript Received July 24, 2010

Stoichiometric $Mn_{0.2}Zn_{0.8}Fe_2O_4$ monodisperse nanoparticles were prepared by the so-called polyol method. The variation of magnetization as a function of magnetic field H (up to ±50 kOe) and temperature (5−320 K) were investigated, for zero-field-cooled (ZFC) and field-cooled (FC) conditions on freshly produced powder. The T variation of the low-field (H = 200 Oe) magnetic susceptibility is characteristic of superparamagnets with a blocking temperature below room temperature. The H variation of the low temperature (T = 5 K) magnetization exhibits a hysteresis loop. The coercivity is weak, about 0.2−0.3 kOe, which is typical of soft-ferrimagnetic materials. The 0 K saturation magnetization and the Curie temperature are found to be 98 emu.g^{-1} and 360 K, respectively. The magnetic properties of the particles are discussed in relation with their chemical composition and their cation distribution in the opportunity of using them as heating mediators for hyperthermia application in cancer therapy. In this aim, the toxicity of the particles was also evaluated by viability assays on human umbilical vein endothelial cells (HUVEC).

Introduction

The use of magnetic MFe_2O_4 spinel ferrite nanoparticles for biological and clinical applications is undoubtedly one of the most challenging research areas in the field of nanomagnetism. They are currently under investigation for several applications, one of the most promising of which is magnetic fluid hyperthermia (MFH).[1−5] The possibility of exploiting these for MFH relies on the heat released by the particles upon application of an alternating magnetic field usually in the $50 < f < 1000$ kHz frequency range when they are dispersed into a fluid. The heat effect on magnetic particles in an alternating magnetic field is considered to be caused by relaxation processes which are the gradual alignment of the magnetic moments during the magnetization process: loss processes during the reorientation of the magnetization[6] or frictional losses if the particle can rotate in an environment of sufficiently low viscosity.[7] The experimental results obtained by many research groups revealed that the heating power strongly depends both on the alternative magnetic field and on the nature of the used particle: their size, size distribution, anisotropy constant, saturation magnetization, and surface modification.[5,8,9] To optimize their suitability for MHF, the size of the magnetic particle core has to be carefully controlled while the interaction of the organic coating with nearby solvent molecules has to be understood.

However, even if very promising clinical trial results were already obtained,[10] some technical problems have still to be conquered. The first of them is concerned with the control of the target temperature in order to reach homogeneous temperature distribution. The second is the

*Corresponding author. E-mail: ammarmer@univ-paris-diderot.fr. Address: Université Paris Diderot−Paris 7 ITODYS, UMR-CNRS 7086 Bâtiment Lavoisier, 15 Rue Jean-Antoine de Baïf, 75205 Paris, France. Tel.: (33)1 57 27 87 62. Fax: (33)1 57 27 72 63.

(1) Brusentsova, T. N. N.; Brusentov, A; Kuznetsov, V. D.; Nikiforov, V. N. *J. Magn. Magn. Mater.* **2005**, *293*, 298.
(2) Kim, D. H.; Lee, S. H.; Kim, K. N.; Kim, K. M.; Shim, I. B.; Lee, Y. K. *J. Magn. Magn. Mater.* **2005**, *293*, 320.
(3) Baldi, G.; Bonacchi, D.; Innocenti, C.; Lorenzi, G.; Sangregorio, C. *J. Magn. Magn. Mater.* **2007**, *311*, 10.
(4) Guedes, M. H. A.; Sadeghiani, N.; Peixoto, D. L. G.; Coelho, J. P.; Barbosa, L. S.; Azevedo, R. B.; Kückelhaus, S.; Da Silva, M. D.; Morais, P. C.; Lacava, Z. G. M. *J. Magn. Magn. Mater.* **2008**, *293*, 283.
(5) Hergt, R.; Andra, W.; d'Ambly, C. G.; Hilger, I.; Kaiser, W. A.; Richter, U.; Schmidt, H. G. *IEEE Trans. Magn.* **1998**, *34*, 3745.
(6) Kneller, E. *Theory of the Magnetization Curve of Small Crystals*; Springer-Verlag: New York, 1966.
(7) Shliomis, M. I. *Sov. Phys. Usp.* **1974**, *17*, 153.
(8) Brusentsov, N. A.; Gogosov, V. V.; Brusentsov, T. N.; Sergeev, A. V.; Jurchenko, N. Y.; Kuznetsov, A. A.; Kuznetsov, O. A.; Shumakov, L. I. *J. Magn. Magn. Mater.* **2001**, *225*, 113.
(9) Rosensweig, R. E. *J. Magn. Magn. Mater.* **2002**, *252*, 370.
(10) Maier-Hauff, K.; Rothe, R.; Scholz, R.; Gneveckow, U.; Wust, P.; Thiesen, B.; Feussner, A.; von Deimling, A.; Waldoefner, N.; Felix, R.; Jordan, A. *J. Neurooncol.* **2007**, *81*, 53.

 Published on Web 09/02/2010

control of the amount of heating material to be applied to the patient. A large heating power of the material is desirable in order to reduce this amount with as low as possible toxicity threshold. So, it becomes crucial to success in producing biocompatible and magnetic monodisperse nanoparticles, stable in physiological media and able to form colloids for in vivo administration. Finally, the Curie temperature of such particles has to be as close as possible to the therapeutically temperature for cancer therapy, namely, 42−47 °C (315−320 K), which allows for self-regulated temperature control in an alternating magnetic field, whereas the saturation magnetization has to be as high as possible at the body temperature, namely, 37 °C (310 K), which allows for great magnetic sensibility.

$Mn_{1-x}Zn_xFe_2O_4$ nanoparticles (MZFOs) are probably the most promising materials. Indeed, they are stable in air and water and are able, due to their reduced size, to form aqueous colloids. They are also assumed to be biocompatible within certain threshold limits. They allow, due to their magnetic tailorability through their chemical composition (zinc content) and cation distribution, very attractive temperature-sensitive magnetic properties. They usually adopt a face centered cubic structure in which the Mn^{2+} and Fe^{3+} paramagnetic ions are located in the tetrahedral (A) and octahedral (B) sites. The substitution of a large part of Mn^{2+} cations by nonmagnetic Zn^{2+} in A sites greatly reduces the resultant magnetization according to the canted ferrimagnetic Yafet-Kittel-like model.[11] However, if Zn^{2+} ions are simultaneously located in A and B sites, the canting is weakened and the magnetization reduction is limited, still leading to suitable saturation magnetization values.[12] Zinc substitution also affects the Curie temperature, T_C, which is closely related to the number of linkages between paramagnetic cations through oxygen anions per formula unit.[13] This number decreases when diamagnetic cations are introduced into the spinel lattice, reducing the T_C value.

We propose to assess the applicability of high Zn-substituted $MnFe_2O_4$ nanoparticles, namely $Zn_{0.8}Mn_{0.2}Fe_2O_4$, prepared by the so-called polyol method which consists of forced hydrolysis of ionic metal salts in a polyol. In the one hand, we focus our experiments on the magnetic properties of these particles in relation with their structure and microstructure, since the heating effect depends strongly on both, while in the other hand we evaluate the toxicity of these particles through in vitro viability assays on human umbilical vein endothelial cell cultures (HUVECs). In vitro cell experiments are well-suited for developing mechanistic models to inform about material development and further in vivo applications. For this purpose we used an MTT assay, which is a colorimetric-based test used to determine cytotoxicity of potential medicinal agents and other toxic materials. Mitochondria represent vulnerable targets for toxic injury because of their crucial role in maintaining cellular structure and function. Notably, mitochondrial damage is a key event in particular matter-induced cytotoxicity.[14] Therefore, we assessed concurrent effects of the magnetic particle on the mitochondrial function and cell viability of endothelial cells.

Experimental Section

1. Chemicals. Iron(III) chloride (PROLABO, 95%), manganese(II) acetate tetrahydrate (Aldrich, >99%), zinc(II) acetate dihydrate (Fluka, >99%), sodium(I) acetate trihydrate (PROLABO, 99%), and bis(2-hydroxy ethyl) ether called also diethyleneglycol (ACROS ORGANICS, 99%).

2. Synthesis. MZFOs were prepared by hydrolysis of manganese acetate, zinc acetate, and iron chloride salts in diethyleneglycol under reflux for at least six hours. An appropriate amount of sodium acetate is added to the mixture. The iron, zinc, and manganese ionic salts concentrations are fixed to 0.20, 0.16, and 0.08 M, respectively, to reach the stoichiometric $Mn_{0.2}Zn_{0.8}Fe_2O_4$ composition. After being cooled to room temperature, powders are separated from the supernatant by centrifugation, washed with water to dissolve NaCl, and then air-dried at 50 °C (323 K).

3. Characterization. Crystal structure of the powder was examined by a Panalytical XperPro diffractometer equipped with a multichannel detector (X'celerator), using a Co K_α radiation ($\lambda = 1.7889$ Å) in the 10−90° 2θ range. The cell parameter and the size of coherent diffraction domain were determined with MAUD software,[15] which is based on the Rietveld method combined with Fourier analysis, well-adapted for broadened diffraction peaks.

The chemical composition is checked by Inductively Coupled Plasma (ICP) analysis at the CNRS Centre of analysis (Vernaison, France).

The size and shape of the particles were determined by JEOL-100-CX II TEM and Jeol-JEM2010-UHR HRTEM microscopes operating at 100 and 200 kV, respectively. One drop of an aqueous suspension of the as-produced particles was deposited on the carbon membrane of the microscope grid for further analysis. The particle size distribution was obtained from transmission electron microscopy (TEM) images using a digital camera and the SAISAM software (Microvision Instruments). The average particle diameter d_p was estimated from following eq 1

$$d_P = \frac{\sum_i n_i d_i^2}{\sum_i n_i d_i} \quad (1)$$

where n_i is the number of particles with d_i diameter (in nanometer). Statistical data were obtained by counting about 400 particles considering a spherical particle shape.

A Quantum Design MPMS-5S SQUID magnetometer was used for magnetic characterization in the temperature range of 4.2−330 K. The thermal ZFC (zero field cooling) and FC (field cooling) susceptibility variation was measured under a static magnetic field of 200 Oe. The isothermal magnetization was also measured by cycling the magnetic field between +50 and −50 kOe at different temperatures. All the measurements were conducted on freshly produced particles mechanically dispersed

(11) Yafet, Y.; Kittel, C. *Phys. Rev.* **1952**, *87*, 290.
(12) Ammar, S.; Jouini, N.; Fiévet, F.; Beji, Z.; Smiri, L.; Molinié, P.; Grenèche, J. M. *J Phys: Condens. Matter* **2006**, *18*, 9055.
(13) Gilleo, M. A. *J. Phys. Chem. Solids* **1960**, *13*, 33.
(14) Hiura, T. S.; Li, N.; Kaplan, R.; Horwitz, M.; Seagrave, J. C.; Nel, A. E. *J. Immunol.* **2000**, *165*, 2703.
(15) Lutterotti, L.; Matthies, S.; Wenk, H. R. *IUCr: Newsl. Commission Powder Diffr.* **1999**, *21*, 14.

in diamagnetic alumina (4.13 wt %) and then slightly compacted into a plastic sampling tube in order to lower the influence of the interparticle interactions and to prevent the physical movement of the particles during the experiments. For comparison, the thermal variation of the FC and ZFC dc-susceptibility was also recorded directly on the as-produced particles.

Extended X-ray Absorption Fine Structure (EXAFS) data were collected at 77 K for the Fe, Mn and Zn K-edges using a transmission mode detection scheme with a Si(111) two-crystals monochromator on the XAFS beamline of the ELLETRA storage ring at the Italian facilities (Trieste). Data were also similarly collected on commercial powdered samples, $ZnFe_2O_4$ (Alfa) and Fe_3O_4 (Prolabo) as standards for Zn and Fe. The samples were ground and homogeneously dispersed in cellulose pellets. EXAFS data were analyzed using the "EXAFS pour le Mac" software package[16] with calculated amplitude and phase shift functions from FEFF7 program.[17]

The ^{57}Fe Mössbauer spectra were recorded in a transmission geometry using a ^{57}Co/Rh γ-ray source. Spectra were obtained at 300 and 77 K in a zero magnetic field and at 11 K in a field of 6 T oriented parallel to the γ-radiation. The sample consists of a thin layer of nanoparticles containing 5 mg of Fe/cm^2. The data were analyzed by a least-squares fitting method using Lorentzian functions. The isomer shift values (δ) are referenced to that of α-Fe at 300 K.

4. Cell Viability Assays. The toxicity of the particles was evaluated by viability assays performed on immortalized human umbilical vein endothelial cells (HUVEC, Eahy926 clone[18]). Cells were cultured and maintained in Dulbecco's modified Eagle Medium (DMEM) supplemented with 10% fetal bovine serum (FBS) and 100 μg mL^{-1} streptomycine and 100 U mL^{-1} penicillin (Gibco, Invitrogen, Cergy-Pontoise, France) at 37 °C in a humidified atmosphere with 5% pCO_2.

Five thousand HUVECs were cultured overnight onto 96-well plates. Afterward, nanoparticles were introduced into their culture medium at 1, 10, and 100 μg mL^{-1} concentrations after quick ultrasonication in serum-free DMEM. Each dose was repeated in triplicate in at least 2 independent experiments. Cells were further incubated for 30 min and 1, 4, 24, 48, and 72 h. Cell viability was assessed using the MTT method according to manufacturer's instructions (3-(4,5-dimethylthiazol-2-yl)-2,5-diphenyl tetrazolium bromide, Sigma, Saint-Quentin-Fallavier, France). Quickly, 1 mg mL^{-1} of MTT reagent was added to 100 μL cell culture medium and further incubated at 37 °C for 4 h. At the end of the incubation period, the medium was replaced by 100 μL of DMSO detergent reagent and absorbance was measured at 570 nm with a standard microplate reader (Multiskan Ex). As the yellow MTT is reduced to purple formazan by cellular enzymes in living cells, quantity of formazan as measured at 570 nm is directly proportional to the number of living cells in culture. The relative cell viability CV (%) related to control wells containing cell culture medium without nanoparticles was calculated by:

$$CV = \frac{[A]_{test}}{[A]_{control}} \times 100 \qquad (2)$$

where $[A]_{test}$ and $[A]_{control}$ are the absorbance of test and control samples, respectively.

Table 1. Chemical Analysis Results of the Prepared Powder; Expected Zn, Mn, and Fe Weight Contents, Calculated Assuming the $Mn_{0.2}Zn_{0.8}Fe_2O_4$ Chemical Formula, Are Given for Indication

Zn (wt %)		Mn (wt %)		Fe (wt %)	
expected	measured	expected	measured	expected	measured
21.9	22.1	4.6	4.9	46.7	48.0

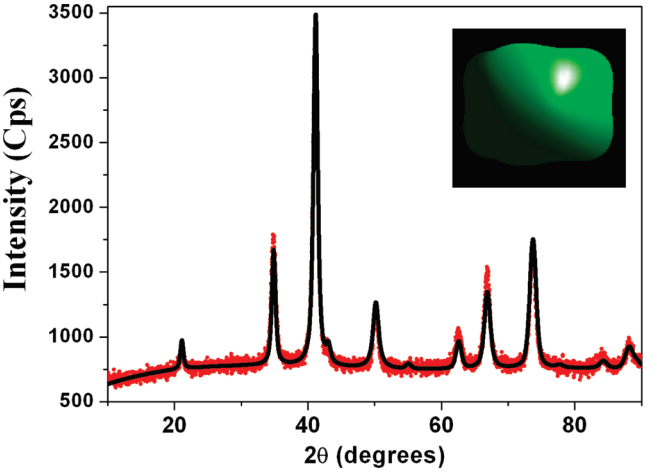

Figure 1. XRD pattern of $Mn_{0.2}Zn_{0.8}Fe_2O_4$ particles refined using MAUD program. The dots correspond to the experimental data and the continued line to the Rietveld fit. The morphology of the coherent diffraction domain inferred from the refinements is given in the inset.

Results

1. Chemical Analysis, Phase Identification, and Morphological Characteristics. Chemical analysis shows that the as-prepared powder sample corresponds to the expected $Mn_{0.2}Zn_{0.8}Fe_2O_4$ composition (Table 1). A small organic contamination resulting from the adsorption of acetate and/or polyol species[19,20] is observed through a nonzero amount of carbon (estimated at about 3 wt %) that decreases significantly with further hot-water washing.

The diffraction pattern plotted in Figure 1 is fully indexed in a pure ferrite spinel phase and the refinement of the lattice parameter was found to be 8.458(4) Å, in good agreement with the expected value for the $Mn_{0.2}Zn_{0.8}Fe_2O_4$ solid solution,[21] whereas the mean size of particles is estimated at about 12 nm assuming a pseudo cubic morphology as illustrated in inset of Figure 1. One may suggest that the prepared MZFO powder is constituted by essentially strain-free and almost cubic in shape nanometer-sized crystals.

The morphology of the particles was examined by low- and high-resolution transmission electron microscopy. TEM micrograph (Figure 2) shows that the particles are almost uniform in size with an average particle diameter of about 8 nm (standard deviation of about 20%) but not exactly spherical in shape. This value is close to the average crystal size previously inferred from XRD analysis, suggesting that the particles are rather single crystals.

(16) Michalowicz, A. *Logiciels pour la Chimie* (*Software for Chemistry*); Société Française de Chimie: Paris, 1991; p 102
(17) Rehr, J. J.; Mustre de Leon, J.; Zabinsky, S. I.; Albers, R. C. *J. Am. Chem. Soc.* **1991**, *113*, 5135.
(18) Edgell, C. J. S.; McDonald, C. C.; Graham, J. B. *Proc. Natl. Acad. Sci. U.S.A.* **1983**, *80*, 3734.
(19) Toneguzzo, P.; Viau, G.; Acher, O.; Fiévet-Vincent, F.; Fiévet, F. *Adv. Mater.* **1998**, *10*, 1032.
(20) Ammar, S; Helfen, A; Jouini, N; Fiévet, F; Rosenman, I; Villain, F; Rosenman, I; Moliné, P; Danot, M *J. Mater. Chem.* **2001**, *11*, 186.
(21) Galasso, F. S. In *International Series of Monographs in Solid State Physics*;Oxford University Press: New York: 1970; Vol. 7.

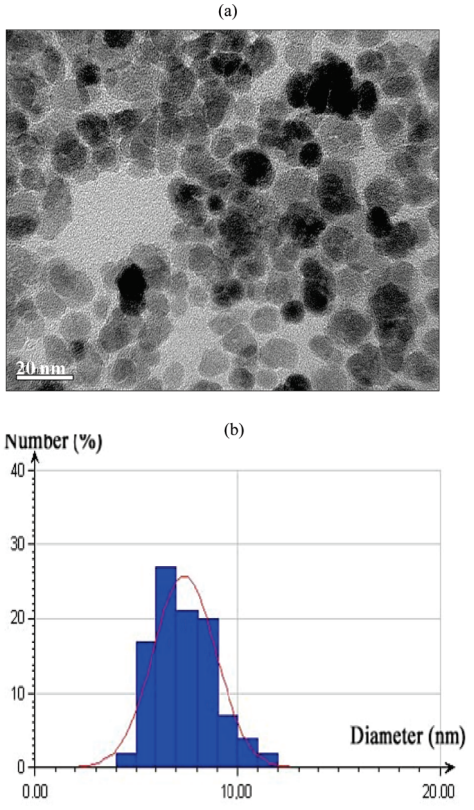

Figure 2. (a) TEM image of a collection of the prepared particles and (b) their size distribution. Note the size distribution is fitted by a log-normal law (red line).

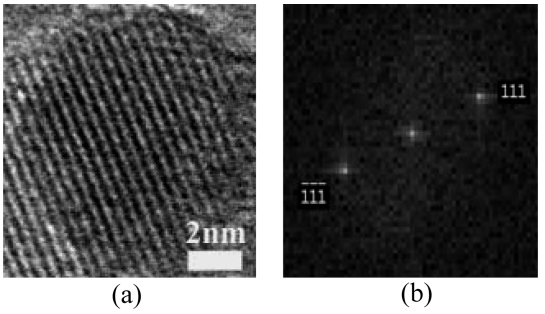

Figure 3. (a) HRTEM image of a representative particle and (b) its FFT pattern (the diffraction plots are indexed according the (111) planes of Mn−Zn ferrite phase).

The HRTEM image (Figure 3) shows fringes corresponding to crystallographic planes of the cubic lattice of the spinel structure. Neither defects such as dislocations or stacking faults, nor amorphous region at the surface were detectable, suggesting thus the high crystalline quality of the particles. The diffraction pattern calculated from the high-resolution images corresponds to the (111) planes of Mn−Zn ferrite phase with a cell parameter of 8.46 Å.

2. Mössbauer and EXAFS Analyses. Both Mössbauer and EXAFS analyses were performed to determine the cation distribution in the spinel lattice in the nanoparticles.

The room-temperature ^{57}Fe Mössbauer spectrum consists of a substantial central quadrupolar doublet with broadened lines (not shown), suggesting the establishment of a superparamagnetic regime of the particles. It can be

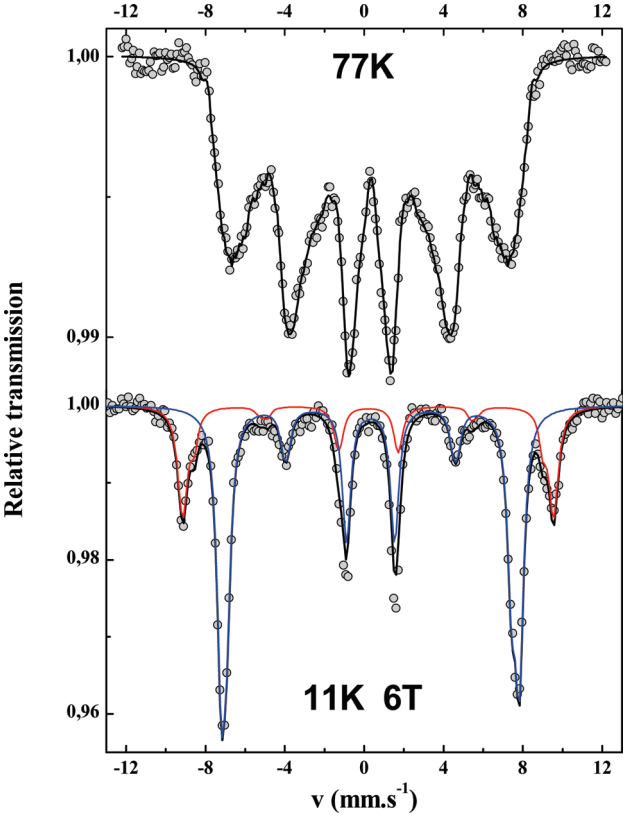

Figure 4. ^{57}Fe Mossbauer spectra recorded at 77 K without an applied field (up) and at 11 K in a 6 T field on the $Mn_{0.2}Zn_{0.8}Fe_2O_4$ particles (down).

reproduced by means of a large quadrupolar splitting (Δ) distribution linearly correlated with a narrow isomer shift (δ), the δ range being characteristic of Fe^{3+}. At 77 K, a magnetic ordering is indicated in the Mössbauer spectrum (Figure 4). A sextet typical of the magnetic hyperfine splitting of the iron ion is observed. The asymmetrical broadening of the absorption lines suggests that the sextet does result from the superposition of two sextets corresponding to tetrahedral (A) and octahedral (B) Fe^{3+} contributions, but the lack of resolution prevents from an accurate estimation of their relative proportion. The application of an external magnetic field allows to split the hyperfine structure into two sextets: we have thus collected a spectrum at 11 K in an applied field of 6 T oriented parallel to the direction of propagation of the γ rays. The recorded spectrum (Figure 4) consists of two sextets, in agreement with a ferrimagnetic structure, whereas the appearance of the second and fifth lines in each sextet suggests a noncollinear spin arrangement. Such a feature may be due to either surface as a consequence of symmetry breaking in the case of confined particles[22] and/or the Yafet-Kittel triangular spin arrangement.[11] Thickness e of the canted magnetic surface which can be derived from the intensities of intermediate lines is estimated at 0.5 nm through the relation $e \approx 0.5r\sin^2\theta$ (where r is the radius of the nanoparticle and θ the angle between the effective field and the γ-beam):[66] the thickness of present nanoparticles

(22) Kodama, R. H.; Berkowitz, A. E.; McNiff, E. J.; Foner, S *Phys. Rev. Lett.* **1996**, *77*, 394.

Table 2. Fitted in Field-Mossbauer Parameters for $Mn_{0.2}Zn_{0.8}Fe_2O_4$ Particles: Isomer Shift Values (IS) Relative to That of α-Fe at 300 K, Quadrupole Shift (2ε), Hyperfine Field B_{hyf}, and Relative Proportion of Each Fe^{3+} Component

site	δ (mm s^{-1}) ± 0.01	2ε (mm.s^{-1}) ± 0.01	B_{eff} (T) ± 2	θ (deg) ± 5	B_{hyp} (T) ± 2	ratio (%) ± 1
A	0.41	−0.01	57.1	24	51.7	27
B	0.51	−0.03	45.6	26	51.1	73

corresponds to about 2 atomic layers. It is important to emphasize that similar size nanoparticles previously prepared by the same chemical route[23] did not exhibit a significant magnetic canted layer because the morphology of the nanoparticles is composed of rather well-defined faces. In the present case pseudo cubic nanoparticles evidenced by X-ray diffraction and confirmed by Transmission Electron Microscopy prevent from the occurrence of such a canted surface. Consequently, we can conclude that the canting does mainly originate from the bulk Yafet-Kittel structure. The refined values of the Mössbauer parameters are listed in Table 2. The A/B population ratio is found to be 0.37. The iron ions distribution estimated from our spectrum corresponds to the formula $(M_{0.46}Fe_{0.54})[M_{0.54}Fe_{1.46}]O_4$ where the round and square brackets correspond to the A- and B- spinel sites, respectively, and M represents indifferently zinc and manganese cations. The measured average canting angles on the magnetic Fe^{3+} moments in A and B sites are lower than those observed in bulk materials. The θ_A and θ_B angles defined by the directions of the effective field for both tetrahedral and octahedral iron components and the γ-beam direction, inferred from in field Mössbauer measurements, are found to be 24 and 26°, respectively, largely lower than those measured on bulk $Mn_{0.2}Zn_{0.8}Fe_2O_4$ materials where Zn^{2+} ions are exclusively located in A sites,[24] which suggests that the structure of the as-prepared particles departs from a direct spinel structure.

The modulus of the Fourier transform (FT) of the total EXAFS data is given in figure 5 at the Zn, Fe and Mn K-edges. The plot of the modulus of the FT is related to the radial distribution function of scatterers around the absorbing atom. By comparison with that of standard $ZnFe_2O_4$ and Fe_3O_4 which adopt a normal and inverse spinel structure, respectively, it is possible to identify the main FT-peaks, at the Fe and Zn K-edges, and by analogy at the Mn one. Three main features are observed:

(i) a decrease in the overall FT intensities for the nanocrystals, with respect to bulk samples;

(ii) the first FT peak, corresponding to the M−O distance, where M is a metallic cation, is clearly split at the Zn and Mn K-edges and exhibits a shoulder at low R-side at the Fe K-edge, suggesting two metal−oxygen distances, the covalent bonds in tetrahedral sites being shorter than electrovalent bonds in octahedral site;

(iii) the second FT peak, corresponding to the metal−metal distance, is split at the Fe, Zn and Mn K-edges, suggesting once again, a distribution of these cations in both, octahedral and tetrahedral sites.

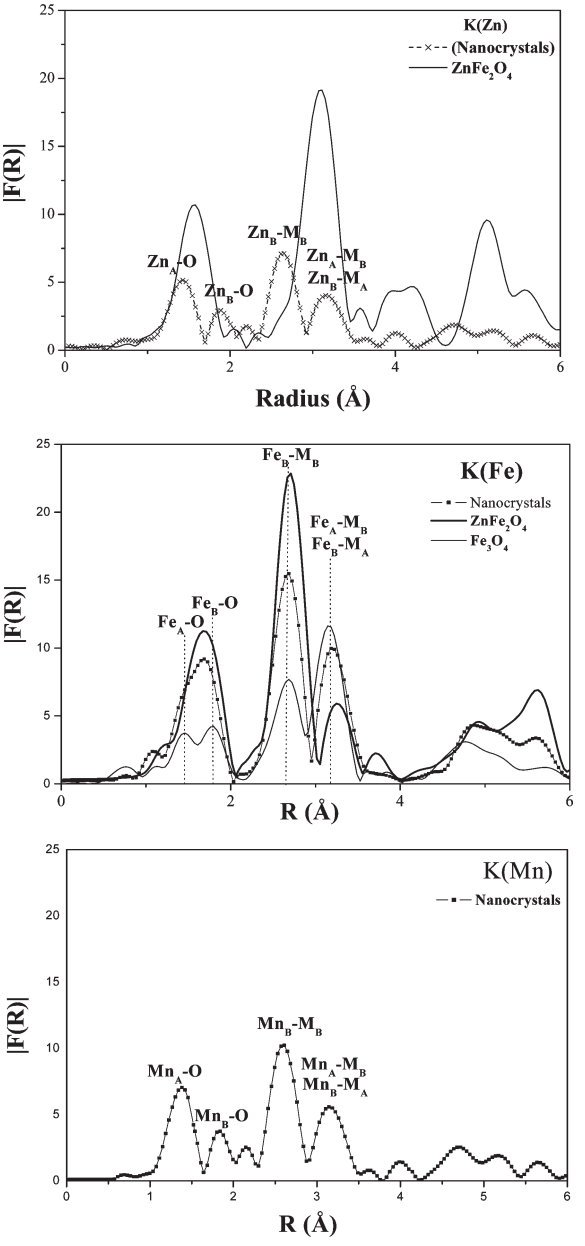

Figure 5. K(Zn), K(Fe), and K(Mn) moduli of the FT experimental EXAFS signals of the $Mn_{0.2}Zn_{0.8}Fe_2O_4$ particles, compared to that of bulk $ZnFe_2O_4$ and Fe_3O_4. The A and B indices correspond to the tetrahedral and octahedral sites occupancy, respectively.

FEFF calculations allow us to establish that multiple scattering contributions can be neglected in the range 0−3 Å for all Fe, Zn, and Mn edges, and suggest that the observed features are related to a transfer of Zn^{2+} from A to B-sites and a reverse transfer of Fe^{3+} and/or Mn^{2+}. This interpretation has been validated by least-squares modeling using single scattering Fe and Zn EXAFS simulation on the filtered first Fe and Zn FT peak corresponding to the Fe−O and Zn−O shell, respectively.

(23) Chkoundali, S.; Ammar, S.; Jouini, N; Fiévet, F; Molinié, P; Danot, M; Villain, F; Grenèche, J. M. *J Phys: Condens Matter* **2004**, *16*, 4357.
(24) Morrish, A. H.; Clark, P. E. *Phys. Rev. B* **1975**, *11*, 278.

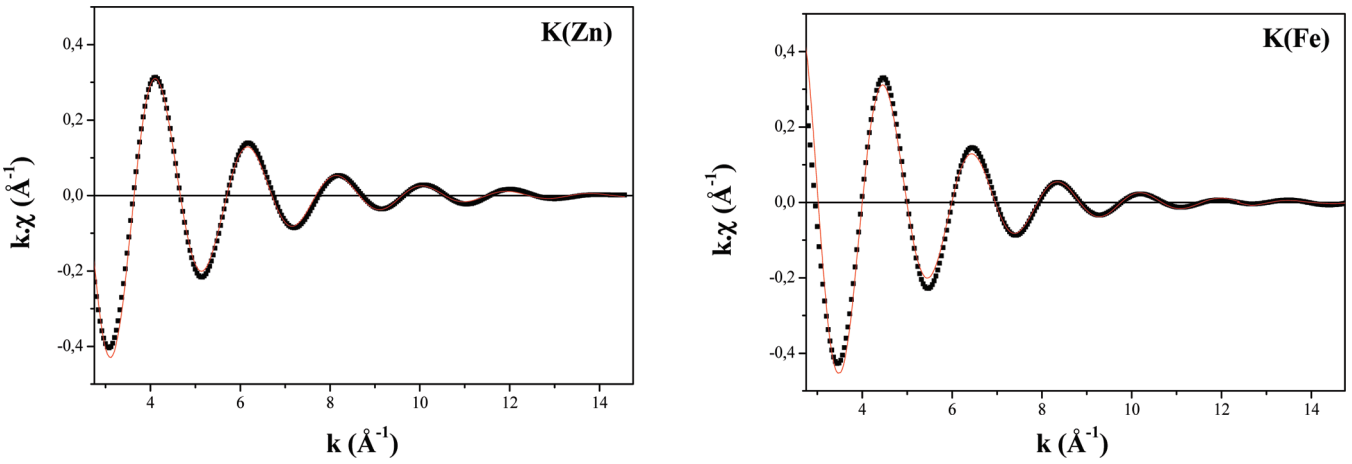

Figure 6. Results of the fit of the inverse Fourier transform of the first peak at the Fe and Zn K-edge for the $Mn_{0.2}Zn_{0.8}Fe_2O_4$ particles.

Table 3. EXAFS Results at the Fe and Zn K-Edges of the $Mn_{0.2}Zn_{0.8}Fe_2O_4$ Particles[a]

	Zn_A-O	Zn_B-O	Fe_A-O	Fe_B-O
N	2.7	2.0	0.9	4.8
R (Å)	1.95	2.05	1.95	2.03
σ (Å)	0.053	0.060	0.057	0.066
ΔE_0 (eV)	6.1	2.7	13.0	7.4

[a] N is the number of backscatterers at a distance R from the central atom and σ the Gaussian Debye−Waller factor associated with R. The energy threshold, E_0, taken at the first inflection of the absorption edge is corrected in the fitting procedure by the ΔE_0 parameter.

Figure 6 illustrates, at the Fe and Zn K-edges, the high quality of the fits. The main structural parameters are listed in Table 3. Using the fitted coordination numbers N of Fe and Zn, the uncertainties being estimated to be about 15%,[16] it is possible to calculate the occupancies of Fe and Zn cations in A and B sites, and consequently Mn cations. Based on the iron A/B atomic ratio established by Mössbauer measurements and confirmed by EXAFS refinements, we find that almost one-third of zinc and one-third of manganese cations are octahedrally coordinated, leading to the following approximated formula: $(Mn_{0.13}Fe_{0.54}Zn_{0.53})[Fe_{1.46}Zn_{0.27}Mn_{0.07}]O_4$.

3. Magnetic Measurements. The magnetic susceptibility, χ, versus T data were measured in ZFC and FC conditions on the as-produced particles (Figure 7a) and on the particles dispersed into a diamagnetic granular alumina matrix to reduce dipolar interaction strength (Figure 7b). In all cases, the magnetic susceptibility shows a net irreversibility, in agreement with the superparamagnetic state previously observed by Mössbauer spectrometry. The ZFC curve measured by cooling the sample in zero field, applying the field at low temperature and then measuring the magnetization while raising the temperature by steps, exhibits a maximum at a temperature commonly referred to the blocking temperature T_B of the sample. T_B is known as the temperature at which the magnetic anisotropy energy barrier of a magnetic single-domain is overcome by thermal activation leading to the fluctuation of the magnetization direction. One can observe that this maximum is broad when the measurements are performed on the as-prepared particles, whereas it is much more narrow when they are performed on the particles dispersed into a solid matrix. The temperature of the ZFC−$\chi(T)$ maximum which becomes better defined is estimated at about 85 K. This suggests that dipolar interactions do exist in the earlier sample while their strength decreases strongly in the latter sample. The FC−$\chi(T)$ curve measured by cooling the sample in a nonzero magnetic field, departs progressively from the ZFC one, when the temperature decreases below the T_B value. Surprisingly, the FC−χ(T) does not continue to rise with decrease in temperature below the blocking temperature as is usually the case for noninteracting superparamagnetic particles[25,26] but exhibits a kind of maximum. Such a feature was previously observed in nonstoichiometric[27] and stoichiometric[12,28] $ZnFe_2O_4$ and high Zn-substituted $CoFe_2O_4$[29,30] and $NiFe_2O_4$[31] nanoparticles. It was related by the different authors to the result of intrinsic strongly canted ferrimagnetic structure.

Below T_B, hysteresis loops were observed with remanence and coercivity which increase when the temperature decreases. At 5 K, their values of 18 emu g^{-1} and 0.2 kOe, respectively (Figure 8), are weak and typical of soft-ferrimagnetic materials. The saturation magnetization is not reached even at a field as high as 50 kOe, suggesting the occurrence of a canting in the magnetic order, as previously suggested by in field Mössbauer spectrometry. Nevertheless, the measured magnetization at 50 kOe is very high, about 88 emu.g^{-1}. The saturation magnetization, $M_{sat,}$ determined by extrapolating the M vs $1/H$ curve to $1/H = 0$, at 5 K is found to be 96 emu g^{-1}. One can note that this value is significantly higher than that of various $Mn_{1-x}Zn_xFe_2O_4$, $x > 0.5$ nanocrystals described in the literature and produced

(25) Makhlouf, S. A.; Parker, F. T.; Berkowitz, A. E. *Phys. Rev. B* **1997**, *55*, R14717.
(26) Walmsley, R. N.; Chantrell, W.; Gore, J.; Maylin, M *J Phys D: Appl Phys* **2000**, *33*, 784.
(27) Hochepied, J. F.; Bonville, P.; Pileni, M. P. *J. Phys. Chem. B* **2000**, *104*, 905.
(28) Grasset, F.; Labhsetwar, N.; Li, D.; Park, D. C.; Saito, N.; Haneda, H.; Cador, O.; Roisnel, T.; Mornet, S.; Duguet, E.; Portier, J.; Etourneau, J. *Langmuir* **2002**, *18*, 8209.
(29) Hochepied, J. F.; Pileni, M. P. *J. Appl. Phys.* **2000**, *87*, 2472.
(30) Basti, H.. Ph.D. Thesis , University Paris 7, Paris, 2010,
(31) Beji, Z.; Ben Chaabane, T.; Smiri, L. S; Ammar, S.; Fiévet, F.; Jouini, N.; Grenèche, J. M. *J. Phys. Solidi Status A* **2006**, *203*, 504.

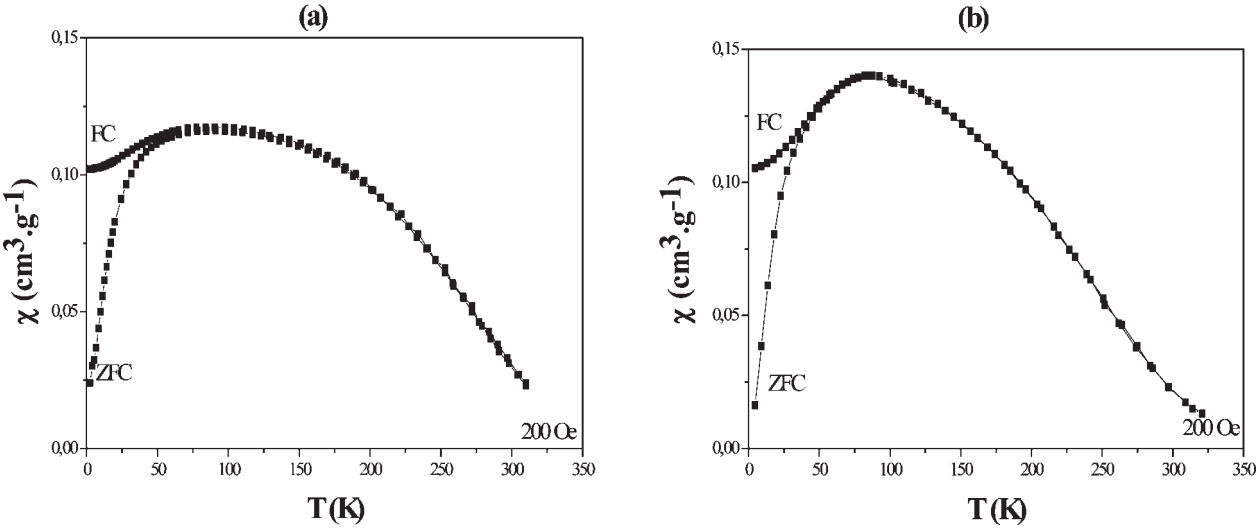

Figure 7. Thermal ZFC- and FC-susceptibility variation measured at 200 Oe on (a) the as-produced $Mn_{0.2}Zn_{0.8}Fe_2O_4$ particles and (b) mechanically dispersed in alumina.

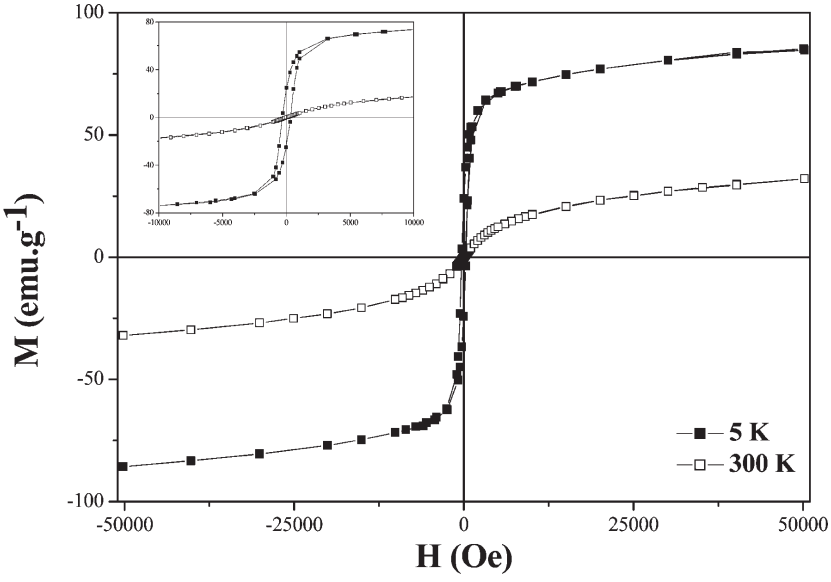

Figure 8. Magnetization $M(H)$ curves measured at 5 and 300 K on the $Mn_{0.2}Zn_{0.8}Fe_2O_4$ particles. A zoom for low field is given in the inset.

by other chemical routes. For instance, values of 19 and 71 emu g^{-1} were reported at 2 and 10 K for 25−40 nm[32] and 10−11 nm[33] sized particles synthesized by reverse micelle technique, respectively. Values of 78 emu g^{-1} and less were reported at 4.2 K for 13 nm sized particles produced by coprecipitation route.[34] Above T_B, the hysteresis behavior disappears. The magnetization value decreases to reach, at 50 kOe, 33 and 30 emu g^{-1} at 300 and 310 K, respectively (Figure 8), because of thermal fluctuations.

The spontaneous magnetization, M_s, measured at 50 kOe is plotted against temperature (Figure 9). The Curie temperature of the particles was estimated through a magnon Bloch type law fitting[35]

$$M_s(T) = M_s(0)\left(1 - \frac{T}{T_C}\right)^{3/2} \quad (3)$$

where $M_s(0)$ is the spontaneous magnetization at 0 K. T_C was found to be about 360 K, higher than the reported value for $Mn_{0.2}Zn_{0.8}Fe_2O_4$ bulk material (T_C = 340 K[36]) but still close to the therapeutically temperature.

4. Toxicity. Cell viability of Human endothelial cells (HUVECs) was estimated, through MTT assay, after MZFOs contact with the cellular medium. Time series investigation showed a dose-dependent reduction of mitochondrial function over 24 h of exposure (Figure 10). Concentrations as low as 1 μg mL^{-1} did not exhibit any significant effects on cell viability as compared to the

(32) Gubbala, S.; Nathani, H.; Koizol, K.; Misra, R. D. K. *Physica B* **2004**, *348*, 317.
(33) Poddar, P.; Srikanth, H.; Morrison, S. A.; Carpenter, E. E. *J. Magn. Magn. Mater.* **2005**, *288*, 443.
(34) Jeyadevan, B.; Tohji, K.; Nakatsuka, K.; Narayanasamy, A. *J. Magn. Magn. Mater.* **2000**, *217*, 99.
(35) Bloch, F. *Z. Phys.* **1931**, *61*, 206.
(36) Smith, S.; Wijn, H. P. J. *Ferrites*; Philips Library: Amsterdam, 1961.

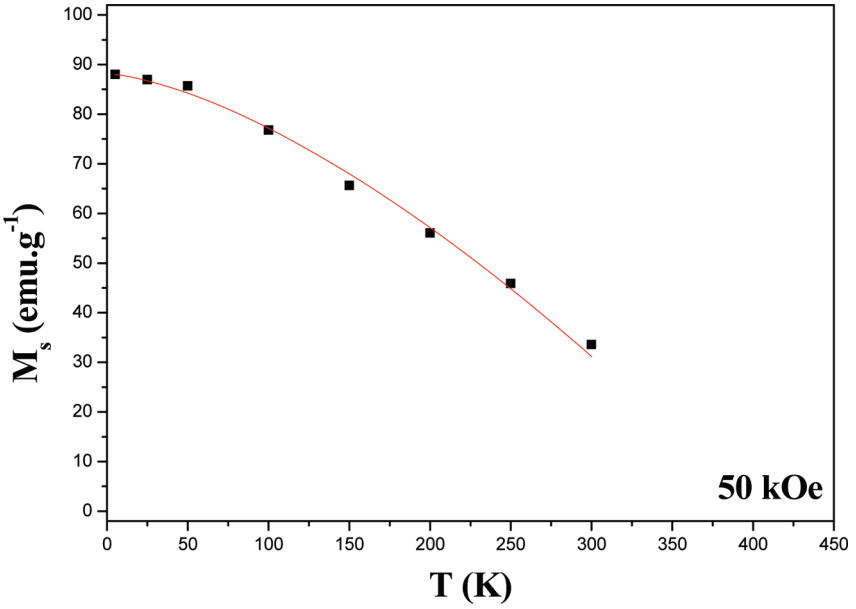

Figure 9. Spontaneous magnetization M_S, measured at 50 kOe, versus T of the $Mn_{0.2}Zn_{0.8}Fe_2O_4$ particles. The continued line corresponds to a $T^{3/2}$ fit.

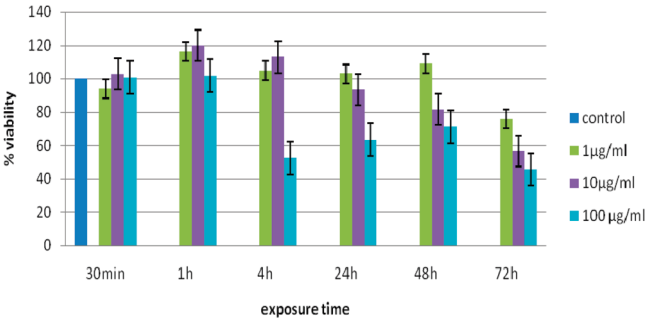

Figure 10. Cell viability of human endothelial cells incubated with $Mn_{0.2}Zn_{0.8}Fe_2O_4$ nanoparticle. The control bar corresponds to the normalized viability of untreated cells. Cells were treated with 1 μg/mL (green bar), 10 μg/mL (purple bar), and 100 μg/mL (turquoise bar) of nanoparticles for 30 min and 1, 4, 24, 48, and 72 h. Toxic effect was considered when the survival rate was below 80%.

control cells. Indeed, the survival rate is maintained above 80% up to 72 h. At a concentration of 10 μg mL^{-1}, the particles caused about 40% of cell death after 72 h of contact time, but no toxic effect occurs from 30 min to 48 h. Strikingly, when used at a concentration of 100 μg mL^{-1}, they originate significant effects on cell viability after 4 h with a decrease of nearly 40% within this dose. Cytotoxicity of ferrite nanoparticles might indeed depend on the particle concentration. High ferrite particle doses ($\geq$100 μg mL^{-1}) have been previously shown to reduce cell proliferation.[37,38]

In conclusion, the MTT assays unveil mitochondrial dysfunction as a key regulator of nanoparticles toxicity. High dose of $Mn_{0.2}Zn_{0.8}Fe_2O_4$ nanoparticles causes a dramatic loss of viability after 4 h of interaction. The MTT assay evaluates the mitochondria activity and therefore can be used as a method to test cell growth as well as cell death.[62] Potential disorder of mitochondria is one of the earliest intracellular events that occur following induction of apoptosis.[63]

Discussion

The possibility of exploiting magnetic ferrite nanoparticles for MFH relies on the heat released by the particles upon application of an alternating magnetic field usually in the $50 < f < 1000$ kHz frequency range when they are dispersed as a magnetic fluid. The heat effect is caused by relaxation processes which are related to the gradual alignment of the magnetic moments during the magnetization process through (i) the internal rotation of the particle's magnetic moment within crystal (Néel mechanism) and (ii) the external rotation of the whole particle in the carrier fluid (Brown mechanism). These losses are characterized by different relaxation times, the shorter time determining the dominant mechanism of relaxation. Fortin et al. showed, in the case of soft ferrimagnetic material, the Néel mechanism accounted for most of the loss power of the particles[39] and then the magneto-thermal properties of the heating agents, namely the magnetic nanoparticles, became quasi-independent of the fluid carrier nature. So when these nanoparticles behave as superparamagnets ($T_B < T < T_C$), the relaxation time τ of the particles to flip their magnetization from one easy direction to its opposite is determined by the ratio of anisotropy energy to thermal energy according to the following equation[6,40,41]

$$\tau = \tau_0 e^{KV/k_B T} \quad (4)$$

where τ_0 is the characteristic relaxation time for a ferrimagnetic material. It is sometimes assumed to be

(37) Jeng, H. A.; Swanson, J. *J. Environ. Sci. Health, A: Tox. Hazard. Subst. Environ. Eng.* **2006**, *41*, 2699.
(38) Pradhan, B.; Majee, S. K.; Batabyal, S. K.; Pal, A. J. *J. Nanosci. Nanotechnol.* **2007**, *7*, 4534.
(39) Fortin, J. P.; Wilhem, C.; Servais, J.; Ménager, C.; Bacri, J. C.; Gazeau, F. *J. Am. Chem. Soc.* **2007**, *129*, 2628.
(40) Chan, D. C. F.; Kirpotin, D. B.; Bunn, P. A. *J. Magn. Magn. Mater.* **1993**, *122*, 374.
(41) Jordan, A.; Wust, P.; Fähling, H.; John, W.; Hinz, A.; Felix, R. *Int. J. Hyperthermia* **1993**, *9*, 51.

about 10^{-10} s[64] and sometimes to be about 10^{-9} s.[39] K measures the effective magnetic anisotropy constant and V the volume of the particles, k_B being the well-established Boltzmann constant. According to the Stoner−Wohlfarth theory of non interacting isotropic and randomly distributed magnetic uniaxial single-domains (nanoparticles), KV is directly dependent on the average T_B value of the nanoparticles:[42]

$$\mathrm{KV} = k_B T_B \ln\left(\frac{\tau_{DC}}{\tau_0}\right) \quad (5)$$

where τ_{DC} measures the DC measurement time ($\sim$ 100 s for a SQUID). Assuming the value of 85 K for T_B, the relaxation time of the particles is, in a first approximation, directly dependent on the T_B value as follows

$$\tau = \tau_0 e^{T_B/T.\ln(\tau_{DC}/\tau_0)} \quad (6)$$

Using eq 6, the τ value of the studied here $Mn_{0.2}Zn_{0.8}Fe_2O_4$ nanoparticles at the body temperature, 310 K, is about 1.95×10^{-7} and 1.04×10^{-6} s, for a τ_0 of 10^{-9} and 10^{-10} s, respectively. Knowing this relaxation time, it becomes possible to determine the optimal applied AC field frequency f ($= \omega/2\pi$) for MHF application. Hergt et al. established that at low frequencies ($\omega\tau \ll 1$), i.e., relaxational losses increase with the square of AC field frequency f while for $\omega\tau \gg 1$ relaxational losses saturate, i.e., these losses become independent of frequency.[5] The transition between these two technical situations takes place near $\omega\tau = 1$. It corresponds in the present case to a f value of about 815 and 153 kHz, depending if we assume that τ_0 is about 10^{-9} or 10^{-10} s, respectively. These values are largely lower than higher technical frequency of appropriate penetration depth of the rf-field in the tissues, namely 10 MHz,[42] and it is also superior to the 50 kHz limit for avoiding neuromuscular electro-stimulation,[43] giving us a large working-frequency window to use the particles described here. The measurement of the thermal dissipation of the particles in the water, induced by an alternating magnetic field of different frequencies (from 100 to 1000 kHz), is in progress. Preliminary results show that, instead of its weakness, the thermal dissipation differs from zero and increases when the applied frequency increases (from about 0.5×10^{-3} to 1.0×10^{-3} K s^{-1} L g^{-1} when the alternative field frequency increases from 100 to 700 kHz, using homemade devices for magnetically induced hyperthermia [[65] and,[39] respectively], on an aqueous colloidal MZFOs' solution). This frequency dependence agrees well with an estimation of the Néel frequency around 815 kHz.

The applicability of the produced MZFOs for MHF is strongly dependent on their magnetic characteristics (see Table 4). Beside their blocking temperature value, the saturation magnetization of the particles is also an important technical parameter. Large magnetization value at working temperature is suitable for in vivo MFH. A higher magnetization suggests a higher specific absorption rate (SAR)[44,46] since SAR has square dependency with the magnetic moment. The M_{sat} values measured at 5, 300, and 310 K on the polyol-made $Mn_{0.2}Zn_{0.8}Fe_2O_4$ nanoparticles are larger than that of similar crystals produced by other chemical routes.[32−34] They are also higher than that of iron oxide particles of less than 10 nm in size produced by conventional aqueous coprecipitation route and widely studied for MFH.[47−50] This enhancement can be partly explained by the highly crystalline quality of the particles. In these particles, the crystallographic particle surface and/or core atomic disorder is minimal (Figure 3a). It can be also explained by their chemical composition and their original cation distribution. Indeed, the introduction of diamagnetic cations into the spinel lattice usually induces a magnetization increase according to the collinear ferrimagnetic Néel theory. When the zinc substitution ratio is large, the ferrimagnetic structure of the particles progresses to a canted structure according to the Yafet-Kittel theory, leading to a magnetization decrease. The spin canting is maximal when Zn^{2+} is exclusively tetrahedrally coordinated. It becomes less important when Zn^{2+} is tetrahedrally and octahedrally coordinated,[12] thus reducing less the total magnetization value of the particle. This irregular distribution of the metal ions in the spinel lattice affects also the Curie temperature value. Whereas large diamagnetic cation, namely Zn^{2+}, concentration favors T_C decrease, a partial transfer of a nonzero number of Zn^{2+} cation from A to B sites and reversely Fe^{3+} and/or Mn^{2+} cations from B to A, can limit the decrease of T_C.[51−53] Indeed, it is well established that T_C is determined by the overall strength of the A−B interactions.[13] Consequently, it is closely related to the number of the linkages between paramagnetic cations, in the present case Fe^{3+} and Mn^{2+}, through oxygen anions per formula unit and also on their distribution over the A and B sites. Usually, when paramagnetic cations of a given spinel site are partly substituted by nonmagnetic ones, the number

Table 4. The main magnetic characteristics of the $Mn_{0.2}Zn_{0.8}Fe_2O_4$ particles

T_B (200 Oe) (K)	H_c (5 K) (kOe)	M_{Sat} (5 K) (emu g^{-1})	T_c (K)
85	0.3	96.0	360

(42) Stoner, E. C.; Wohlfarth, E. P. *Philos. Trans. R. Soc. London, Ser. A* **1948**, *240*, 599.
(43) Mornet, S.; Vasseur, S.; Grasset, F.; Duguet, E. *J. Mater. Chem.* **2004**, *4*, 2161.
(44) Hill, D. A. *Bioelectromagnetics* **1985**, *6*, 33.
(45) Pollert, E; Knızek, K; Marysko, M; Kaspar, P; Vasseur, S; Duguet, E *J. Magn. Magn. Mater*. **2007**, *316*, 122.
(46) Prasad, N. K.; Rathinasamy, K; Panda, D; Bahadur, D *J. Mater. Chem*. **2007**, *17*, 5042.
(47) Hergt, R.; Hiergeist, R.; Hilger, I.; Kaiser, W. A.; Lapatnikov, Y.; Margel, S.; Richter, U. *J. Magn. Magn. Mater*. **2004**, *270*, 345.
(48) Sonvico, F.; Mornet, S.; Vasseur, S.; Dubernet, C.; Jaillard, D.; Degrouard, J.; Hoebeke, J.; Duguet, E. *Bioconjugate Chem*. **2005**, *16*, 1181.
(49) Maier-Hauff, K.; Rothe, R.; Scholz, R.; Gneveckow, U.; Wust, P.; Thiesen, B.; Feussner, A.; Von Deimling, A.; Waldoefner, N.; Felix, R.; Jordan, A. *J. Neurooncol*. **2007**, *81*, 53.
(50) Johannsen, M.; Gneveckow, U.; Thiesen, B.; Taymoorian, K.; Cho, C. H.; Waldöfner, N.; Scholz, R.; Jordan, A.; Loening, S. A.; Wust, P. *Eur. Urol*. **2007**, *52*, 1653.
(51) Rath, C.; Anand, S.; Das, R. P.; Sahu, K. K.; Kulkarni, S. D.; Date, S. K.; Mishra, N. C. *J. Appl. Phys*. **2002**, *91*, 2211.
(52) Auzans, E.; Zins, D.; Blums, E.; Massart, R. *J. Mater. Sci*. **1999**, *34*, 1253.
(53) Morrish, A. H.; Li, Z. W.; Zhou, X. Z. *J. Phys. C*. **1997**, *1*, 513.

of magnetic active linkages decreases. The internal energy required to offset the spin alignment decreases also and the Curie temperature is expected to fall. In our crystalline nanoparticles, 80% of the paramagnetic divalent cations are substituted by diamagnetic zinc ones, but these diamagnetic cations are located on the two A and B sites, limiting thus this T_C reduction.

T_C is an important parameter to design efficient heating mediators for MFH. It measures the temperature at which the ferro- or ferrimagnetic materials loss their magnetic ordering, thus they do not convert electromagnetic energy into heat. T_C is therefore the maximal temperature reachable by magnetic particles. Tuning the Curie temperature at a value just above the treatment temperature would be the smartest way to control the temperature in the human body, avoiding local overheating, which may damage safe tissue. The estimated T_C value from the Bloch-law fit of the MZFO particles under study is of 360 K, namely 87 °C (Figure 9). This value is somewhat higher than the reported one for bulk ferrite and also higher than the desired therapeutically temperature. Nevertheless, it remains largely lower than the T_C of iron oxide nanoparticles (SPIO and MION), namely 858 K, the most studied systems for MFH application[54] and closer than the T_C of lanthanum manganese based perovskite particles (of some tens of nanometers in size), namely 352 K for 52 nm sized $La_{0.75}Sr_{0.25}MnO_3$ (LSMOs) particles,[45] the alternative studied systems.[45,55,56] The last system suffers from two major inconvenients for in vivo application: first their relatively large average crystal size (usually higher than 20 nm), which limits the ability of the LSMOs particles to cross the overall endovascular epithelium barrier, and second their relatively important intrinsic toxicity, which limits the safely doses of the LSMOs particles to be addressed to human bodies (LSMO is found biocompatible only for limited dose of 660 μg per mL of culture media[57]).

Obviously, the as-prepared MZFO particles have excellent features. They are small enough to cross overall endovascular epithelium barrier and they do not exhibit severe toxicity as established by preliminary MTT assay after nanoparticles contact with HUVECs. MTT assay is a widely used test to evaluate cytotoxicity of various molecules and drugs in cell culture,[57] so that it is often used alone for the evaluation of in vitro cytotoxicity, particularly that of nanoparticles cytotoxicity.[58,59] Comparing MTT assay results performed on other substituted ferrite nanoscale materials ($ZnFe_2O_4$,[59] $NiFe_2O_4$,[60] $CoFe_2O_4$,[60] $MnFe_2O_4$,[61] ...) to that obtained on our particles the latter are much less cytotoxic than the former, at least for period of time shorter than 24 h. For instance, the endothelial cell viability ratio was only 55% at the dose of 100 μg mL^{-1} after 24 h of contact time with $NiFe_2O_4$ nanoparticles of some nanometers in size,[60] whereas it is about 70% after 48 h of contact with the here-studied MZFO particles.

Conclusion

Crystalline $Mn_{0.2}Zn_{0.8}Fe_2O_4$ nanoparticles were successfully prepared using forced hydrolysis in diethyleneglycol. This chemical route allows us to directly prepare nanoparticles with very uniform size and morphology without any further selection process. They behave clearly as superparamagnets at room temperature and as ferrimagnets at low temperature. EXAFS and in-field Mössbauer measurements reveal a departure from the thermodynamically stable spinel structure, with a nonzero number of Zn^{2+} ions located in octahedral sites. The magnetic properties are strongly influenced by such a cation distribution in the nanoparticles. The room temperature saturation magnetization and the Curie temperature are suitable for MFH application. Moreover, human endothelial cells (HUVECs) submitted to MTT viability assay after nanoparticles contact have shown that the cytotoxicity of these particles depend on the ferrite concentration. It appears that lower doses (1−10 μg mL^{-1} nanoparticle concentration) might be safely used without alteration of cell viability at least for the first 48 h. MFH studies are in progress on these promising agents. The specific loss power of the particles in an alternating magnetic field (from 100 to 1000 kHz) will be calorimetrically calculated and the possible toxicity mechanisms, such as oxidative stress or lipid peroxidation and particle localization within the cell, will be evaluated.

Acknowledgment. The CMCU France-Tunisia Cooperation Research Program is thanked for financial support. The authors are indebted to Dr. Y. Li for the access to the SQUID and to Dr Luca Olivi for his help at the ELLETRA synchrotron ring of Trieste. They are also indebted to Drs. Julian Carey and Florence Gazeau for the preliminary in vitro hyperthermia measurements.

(54) Zheng, M.; Wu, X. C.; Zou, B. S.; Wang, Y. J. *J. Magn. Magn. Mater.* **1998**, *183*, 152.
(55) Moroz, P.; Jones, S. K.; Gray, B. N. *Int. J. Hyperthermia* **2002**, *18*, 267.
(56) Vasseur, S.; Duguet, E.; Portier, J.; Goglio, G.; Mornet, S.; Hadova, E.; Knızek, K.; Marysko, M.; Veverka, P.; Pollert, E. *J. Magn. Magn. Mater.* **2006**, *302*, 315.
(57) Prasad, N. K.; Hardel, L.; Duguet, E.; Bahadur, D. *J. Magn. Magn. Mater.* **2009**, *321*, 1490.
(58) Berridge, M. V.; Herst, P. M.; Tan, A. S. *Biotechnol. Annu. Rev.* **2005**, *11*, 127.
(59) Bhirde, A. A.; Patel, V.; Gavard, J.; Zhang, G.; Sousa, A. A.; Masedunskas, A.; Leapman, R. D.; Weigert, R.; Gutkind, J. S.; Rusling, J. F. *ACS Nano* **2009**, *3*, 307.
(60) Tomitaka, A.; Hirukawa, A.; Yamada, T.; Morishita, S.; Takemura, Y. *J. Magn. Magn. Mater.* **2009**, *321*, 1482.
(61) Giri, J; Pradhan, P; Somani, V; Chelawat, H; Chhatre, S; Banerjee, R; Bahadur, D *J. Magn. Magn. Mater.* **2008**, *320*, 724.
(62) Song, M. M.; Song, W. J.; Bi, H.; Wang, J.; Wu, W. L.; Sun, J.; Yu, M. *Biomaterials* **2010**, *31*, 1509.
(63) Han, J; Goldstein, L. A.; Gastman, B. R.; Rabinowich, H *J. Biol. Chem.* **2006**, *281*, 10153.
(64) Zysler, R. D.; Winkler, E. *IEEE Nanotechnol.* **2007**, *18*, 158001.
(65) Lacroix, L.-M.; Carrey, J.; Respaud, M. *Rev. Sci. Instrum.* **2008**, *79*, 1.
(66) Tronc, E.; Prené, P.; Jolivet, J.-P.; Dormann, J.-L.; Greneche, J.-M *Hyperfine Interact.* **1997**, *112*, 97.